Title Page

Matrix Metalloproteinase-9 controls structural synaptic plasticity via BDNF-dependent signaling

Authors/affiliations

Diana Legutko[1,2], Bożena Kuźniewska[1,3], Katarzyna Kalita[1], Ryohei Yasuda[2,*], Leszek Kaczmarek[1,*] , Piotr Michaluk[1,*]

[1]BRAINCITY, Laboratory of Neurobiology, The Nencki Institute, 02-093 Warsaw, Pasteura 3, Poland

[2]Max Planck Florida Institute for Neuroscience, 1 Max Planck Way, Jupiter, Florida 33458, USA

[3]Current address: Department of Animal Physiology, Institute of Functional Biology and Ecology, Faculty of Biology, University of Warsaw, Miecznikowa 1, 02-096, Warsaw, Poland

Contact info

*Correspondence: Piotr Michaluk, p.michaluk@nencki.edu.pl; Ryohei Yasuda, ryohei.yasuda@mpfi.org; Leszek Kaczmarek, l.kaczmarek@nencki.edu.pl

Abstract

Structural long-term potentiation (sLTP), an activity-dependent growth of dendritic spines that harbor excitatory synapses, is a major form of synaptic plasticity in learning and memory processes. The spine enlargement is influenced by the extracellular matrix and its proteolytic enzymes, among which matrix metalloproteinase 9 (MMP-9) is a prominent example. Here, we utilized two-photon microscopy and two-photon glutamate uncaging to demonstrate that MMP-9 activity is essential for sLTP and is rapidly (~seconds) released from dendritic spines in response to synaptic stimulation. MMP-9 has been postulated to play a pivotal role in the maturation of brain-derived neurotrophic factor (BDNF), a major protein involved in LTP that acts on TrkB receptor. We show that chemically or genetically inhibiting MMP-9 impairs TrkB activation, as measured by fluorescence lifetime imaging microscopy of FRET sensor. Furthermore, we provide evidence for in vitro cleavage of proBDNF into mature BDNF by MMP-9. Our findings point to autocrine mechanism of action of MMP-9 through BDNF maturation and TrkB activation during sLTP.

Keywords

Synaptic plasticity/Exocytosis/pHluorin/proteolysis/BDNF/MMP-9/dendritic spine/FRET

Introduction

Synaptic plasticity, the ability of synapses to modify their strength in response to their activity, is a fundamental process that underlies learning and memory. Long-term potentiation (LTP) is widely considered to be a cellular model of synaptic plasticity, and it has been extensively studied predominantly on excitatory synapses located on small neuronal protrusions, dendritic spines (Nicoll, 2017). Synaptic strength corresponds, among other factors, to the number of AMPA (α-amino-3-hydroxy-5-methyl-4-isoxazolepropionic acid) receptors. After the LTP induction, AMPA receptors are rapidly inserted into the spine (Patterson *et al*, 2010; Penn *et al*, 2017; Shi *et al*, 1999) thus increasing the strength of a synaptic connection between two neurons. One of the manifestations of LTP is a structural change of dendritic spine morphology, where upon stimulation the spine increases its volume (Matsuzaki *et al*, 2004). To date, multiple molecular pathways have been identified that regulate synaptic plasticity (Hayashi, 2022), including the extracellular matrix (ECM), cell adhesion molecules, neurotrophic factors, and proteolytic enzymes that can process those molecules, with the matrix metalloproteinases (MMPs) serving as particularly prominent proteases (Wiera & Mozrzymas, 2021).

Among the MMPs, zinc-dependent endopeptidases, MMP-9 has emerged as a key player in regulating synaptic plasticity. Research on its involvement in LTP has been ongoing for almost two decades (Nagy *et al*, 2006; Okulski *et al*, 2007; Gorkiewicz *et al*, 2010, 2015; Lebida & Mozrzymas, 2017; Huntley, 2012; Vafadari et al., 2016). MMP-9 is considered one of the essential factors for the maintenance of LTP (Nagy *et al*, 2006) and is crucial for structural plasticity by contributing to a sustained increase of dendritic spines volume evoked by LTP (Wang *et al*, 2008). Upon stimulation, MMP-9 is released from a postsynaptic neuron to the extracellular space, where it can cleave several protein targets (Michaluk *et al*, 2007; Bajor *et al*, 2012; Wiera & Mozrzymas, 2021; Van Der Kooij *et al*, 2014; Ethell & Ethell, 2007; Peixoto *et al*, 2012). Notably, the proteolytic activity is tightly controlled by MMP-9 endogenous inhibitor, Tissue Inhibitor of Metalloproteinase-1 (TIMP-1) (Magnowska *et al*, 2016).

Several studies demonstrated that MMPs including MMP-9 plays a critical role in the maturation of brain-derived neurotrophic factor (BDNF) by processing its precursor form (proBDNF) to mature form (mBDNF) (Lee *et al*, 2001; Hwang *et al*, 2005; Mizoguchi *et al*, 2011; Niculescu *et al*, 2018). ProBDNF is a potent inhibitor of synaptic plasticity, while mBDNF is essential for maintenance of LTP (Kang *et al*, 1997; Lohof *et al*, 1993; Hedrick *et al*, 2016; Monteggia *et al*, 2004; Harward *et al*, 2016). mBDNF promotes synaptic plasticity through the activation of its receptor, tropomyosin receptor kinase B (TrkB) that triggers multiple downstream signaling pathways, including the mitogen-activated protein kinase (MAPK), phospholipase Cγ (PLCγ) and phosphoinositide 3-kinase (PI3K) pathways that are known to be pivotal for the induction and maintenance of synaptic plasticity (Cunha *et al*, 2010).

Despite significant progress in our understanding of the role of MMP-9 in synaptic plasticity, a number of questions remain unanswered. In particular, the kinetics of MMP-9 release and proteolytic action, especially in conjunction with proBDNF activation, is unknown. Depending on the report and protocol used, MMP-9 release has been shown to be as early as 5 minutes upon neuronal stimulation (Michaluk *et al*, 2007) through 15–30 minutes (Nagy *et al*, 2006), and up to 1 hour (Nagy *et al*, 2006, 2007; Bozdagi *et al*, 2007). In the studies where MMP-9 was applied externally as a recombinant protein, it was usually incubated for either 30 (Michaluk *et al*, 2011; Wang *et al*, 2008) or 40 minutes with the cultured neurons (Magnowska *et al*, 2016) to cause morphological change of dendritic spines. In comparison, BDNF, which can be released in pro- and mature-form, has been shown to be secreted rapidly (within seconds) upon increase in K^+ concentration (Dean *et al*, 2009), theta-burst stimulation (Matsuda *et al*, 2009) or sLTP-inducing glutamate uncaging (Harward *et al*, 2016). Additionally, it has been shown that TrkB activation is also almost immediate, reaching the maximum within 1 minute from the onset of stimulation (Harward *et al*, 2016). If MMP-9 activity indeed causes maturation of proBDNF and leads to TrkB activation (Hwang *et al*, 2005; Mizoguchi *et al*, 2011; Niculescu *et al*, 2018), both proteins must coincide in space and time around a dendritic spine. This hypothesis could address a long-standing debate about which enzymes process proBDNF to mBDNF and in which compartments it occurs (Sasi *et al*, 2017). Hence, it is essential to understand the spatiotemporal dynamics of MMP-9 action at the level of single dendritic spines.

This report provides insights into the kinetics of MMP-9 release and activation of TrkB receptors during LTP-evoked structural plasticity. In order to pinpoint the dynamic processes of structural plasticity, protein release, and receptor activation, we have used two-photon imaging, 2-photon fluorescence lifetime imaging microscopy (2pFLIM) to measure Förster Resonance Energy Transfer (FRET) sensor of TrkB, and 2-photon glutamate uncaging on individual dendritic spines (Colgan *et al*, 2018; Tu *et al*, 2020; Chang *et al*, 2019; Harward *et al*, 2016). These techniques allowed us to test how MMP-9 influences structural LTP (sLTP) evoked by glutamate uncaging. We observe MMP-9 release upon sLTP and its effect on TrkB activation. Moreover, in a cell-free assay, we confirm proBDNF cleavage to mBDNF by MMP-9. Overall, our results indicate that both MMP-9 and BDNF are released from stimulated spines, leading to autocrine TrkB activation, and support the hypothesis that rapid maturation of BDNF may occur in the extracellular space upon stimulation.

Results

Spine-head enlargement during sLTP depends on MMP-9 activity

Previous studies have shown that dendritic spine volume and shape correlates with the size of the synapse (Borczyk *et al*, 2019; Vardalaki *et al*, 2022), number of synaptic AMPA-type glutamate receptors (Matsuzaki *et al*, 2001; Shi *et al*, 1999). Therefore, in this study, we focused on dendritic spine volume as a proxy of synaptic plasticity (Tønnesen & Nägerl, 2016). Pyramidal neurons of CA1 subfield of the hippocampus were transfected in organotypic culture using a biolistic method with a plasmid encoding GFP. Successfully transfected neurons were imaged using two-photon microscope. During sLTP stimulation (see Methods and Harward *et al*, 2016), uncaging of 4-methoxy-7-nitroindolinyl (MNI)–glutamate caused rapid and transient three- to four-fold spine volume increase, which subsequently stabilizes at an elevated level, typically ranging from 150-200% of its original size. This sustained phase starts around 8 minutes after stimulation (Fig. 1A-C). Similarly to previous studies, the spine volume change was assessed as a $\Delta F/F_0$ of GFP fluorescence for individual spines in time (Harward *et al*, 2016; Hedrick *et al*, 2016) (see Methods).

To test if MMP-9 activity is necessary for sLTP, we first used a chemical inhibitor of MMP-9 and MMP-13 (Inhibitor I, 5 μM; Figure 1C) and compared the effects with the vehicle (DMSO) control. We assessed spine head volume at three time intervals of sLTP: the transient phase (1-3 minutes after the onset of uncaging), and the sustained phase (9-11 minutes and 15-20 minutes after the uncaging). Presence of Inhibitor I significantly diminished spine volume increase in all phases (Fig 1C, 1D). Therefore, MMPs (including MMP-9) activity appears to be important both during the induction and maintenance of sLTP (as described before).

There are over twenty MMPs with overlapping substrate specificity (Fields, 2015; Cieplak & Strongin, 2017) and there are no fully specific, commercially available inhibitors for MMP-9. Therefore, to further test the involvement of the protease in sLTP, we have used hippocampal slice cultures prepared from MMP-9 KO mice and their WT littermates (Fig 1E, 1F). Unlike chemical inhibitors, MMP-9 KO significantly reduced spine volume change only during the transient phase of sLTP (1-3 min, Fig 1F), but not during the sustained phase. These results suggest that MMP-9 acts rapidly (within 1-3 min) on biochemical processes leading to sLTP.

MMP-9 release during sLTP

The proteolytic activity of MMP-9 in neuronal tissue is tightly controlled on many levels, from transcription, through local translation, release, and inhibition by TIMP-1 (Michaluk *et al*, 2007; Dziembowska *et al*, 2012; Magnowska *et al*, 2016; Szklarczyk *et al*, 2002; Vafadari et al., 2016). However, the exact moment of MMP-9 secretion is unknown during LTP. Our previously published results have shown an increase of MMP-9 level in extracellular neuronal culture medium 5 minutes post neuronal stimulation (with no earlier time-points investigated, see: Michaluk *et al*, 2007; Stawarski *et al*, 2014), yet many studies indicate that mBDNF has to be present during LTP induction to maintain plasticity (Pang *et al*, 2016; Harward *et al*,

2016). If the molecular mechanism of MMP-9 signaling affects the maturation of proBDNF and activation of TrkB, MMP-9 secretion has to be as fast as the release kinetics reported for BDNF (Dean *et al*, 2009; Matsuda *et al*, 2009; Harward *et al*, 2016). To verify if MMP-9 is released from dendritic spines in an activity-dependent manner, we developed pH-sensitive green fluorescent protein (superecliptic pHluorin, SEP) (Miesenböck *et al*, 1998) fused to C-terminus of hemopexin domain of proteolytically inactive mouse MMP-9. Cells in hippocampal organotypic cultures were co-transfected with the MMP9-SEP and mCherry (the latter for the visualization of dendritic spine morphology; Figure 2A-B). To study MMP-9 release during sLTP, we imaged dendritic spines of CA1 pyramidal neurons with 2-photon microscopy at 7.8 frames per second, while stimulating neurons with glutamate uncaging (0.49 Hz or 16 frames, 30 times).

MNI-glutamate uncaging caused an increase in mCherry fluorescence, indicative of spine volume enlargement during sLTP protocol (Fig. 2C). Observation of corresponding MMP-9-SEP fluorescence showed an increase in signal restricted to the stimulated spine (Fig. 2B, 2D), suggesting the release of MMP-9. In order to explore if the MMP-9 release is NMDAR (N-methyl-D-aspartate receptor)-dependent, we applied sLTP protocol in the presence of NMDAR antagonist AP5. This manipulation abolished SEP fluorescence increases during stimulation. Similarly, when the cells were co-transfected with tetanus toxin light chain (TeTx), which blocks the synaptobrevin-dependent exocytosis (Link *et al*, 1992; Harward *et al*, 2016), we did not observe the SEP fluorescence increases during sLTP protocol (Fig. 2D). Therefore, we concluded that synaptic release of MMP-9 requires its exocytosis and is NMDAR-dependent.

To further assess the fast kinetics of MMP9 releases after each uncaging pulse, we divided imaging data into blocks of 16 frames (corresponding to uncaging intervals, 2.048 s), and stacked them in such a way that the uncaging pulse was always applied during the second row of the block (Fig. 2E). Then, the fluorescence data were normalized to the first two averaged rows in each block. This procedure allowed us to visualize the averaged fluorescence changes normalized to fluorescence before uncaging (averaged over 2 frames) as a heatmap (Fig 2E). The resulting image suggests that fluorescence increases appear after the second uncaging pulse and diminishes after the 22nd uncaging pulse (Figure 2E).

In order to study if the increases in MMP9-SEP fluorescence were a result of pH changes associated with MMP9 release, we performed the same experiments using an analogous fusion protein to MMP9-SEP, but with pH-stable form of GFP, Gamillus (Shinoda *et al*, 2018). We did not observe a fluorescence increase in the heatmap from MMP9-Gamillus (Fig. 2F).

To better visualize the rapid release of MMP-9 upon uncaging, we have averaged relative fluorescence for the 2-18 uncaging pulses and plotted them as a function of time, together with the corresponding fluorescence of mCherry (Fig. 2G, 2H). In the mCherry channel, we observed a slow fluorescence increase corresponding to spine volume change. MMP9-SEP fluorescence showed a much faster onset, suggesting a rapid release of MMP9 in response to

each uncaging pulse. MMP9-Gamillus, however, showed signals similar to mCherry (Fig. 2I, 2J). Therefore, these results further support a fast release of MMP-9 at the synapses undergoing sLTP.

TrkB activation depends on MMP-9 activity

Previous studies suggested proBDNF to be a potential target for MMP-9 proteolytic activity that leads to maturation of the neurotrophic factor and activation of TrkB (Hwang *et al*, 2005; Martinelli *et al*, 2021; Niculescu *et al*, 2018; Kaminari *et al*, 2017; Mizoguchi *et al*, 2011). Given that our and other results indicate that both BDNF and MMP-9 are rapidly released upon synaptic stimulation, we hypothesized that MMP-9 took part in the maturation of BDNF. To test this hypothesis, we transfected neurons in hippocampal organotypic cultures with a TrkB FRET sensor made of TrkB fused with GFP and SH2-domain of PLC-delta fused with a pair of mCherry proteins (Harward et al., 2016). Then, we measured TrkB activation (Harward *et al*, 2016) during uncaging-evoked sLTP (Fig. 3B) in the presence of either Inhibitor I or DMSO for control (Fig. 3C, 3D). Inducing sLTP with glutamate uncaging decreased fluorescence lifetime of GFP and increased the calculated binding fraction between TrkB and SH2-domain of the sensor (Fig 3A, 3C), indicating the activation of TrkB (Fig. 3B). Inhibitor I significantly attenuated TrkB activation in comparison to DMSO after the sLTP induction in both transient phase and sustained phases of sLTP (Fig. 3D) indicating that MMP-9 activity is most probably involved in TrkB activation.

To further test if MMP-9 is necessary for TrkB activation, we used hippocampal organotypic cultures prepared from MMP-9 KO mice and their WT littermates (Fig. 3E), and measured TrkB activation with the TrkB sensor. Similarly to the application of Inhibitor I, MMP-9 KO influenced TrkB activity during both transient and sustained phases of structural plasticity. These results demonstrate that MMP-9 is required for both transient and sustained activation of BDNF receptor following repeated glutamate uncaging evoking sLTP.

Finally, we examined if MMP-9 can cleave proBDNF into mBDNF in a cell-free assay. To do this, we incubated a recombinant proBDNF with recombinant active MMP-9 overnight at 37°C in a reaction buffer (see Methods). As a control, we used recombinant inactive mutant (E402A) of MMP-9 or a buffer without MMP-9 (Michaluk *et al*, 2011). The cleavage of proBDNF was quantified by Western blot, using anti-BDNF antibody recognizing both (pro- and mature-form). Incubation with active MMP-9, but not with mutant MMP-9, causes cleavage of proBDNF (Fig 3G). These results indicate that MMP-9 cleaves proBDNF into mBDNF.

Discussion

In this report, we demonstrate that: (i) MMP-9 inhibition impairs structural synaptic plasticity (sLTP) evoked by repetitive stimulation by glutamate uncaging, (ii) MMP-9 is rapidly, within seconds, released from the dendritic spines, (iii) MMP-9 inhibition impairs activation of BDNF receptor TrkB, and (iv) MMP-9 partially cleaves proBDNF to produce its mature form, known to activate TrkB and evoke structural synaptic plasticity. In aggregate, these results demonstrate a mechanistic link between MMP-9 and BDNF in controlling synaptic plasticity.

The MMP-9 effects were evident during sustained phase of sLTP (9-11 or 15-20 min post-stimulation), and even more robustly during the transient phase (1-3 min post-stimulation). The application of MMP-9/-13 Inhibitor I and its effect on sLTP (Fig. 1C, 1D) at the sustained phase of sLTP is in agreement with previously published electrophysiology and imaging data (Nagy *et al*, 2006; Wang *et al*, 2008; Gorkiewicz *et al*, 2015; Wiera *et al*, 2013). However, in slice cultures prepared from MMP-9 KO animals, we did not observe the influence of knockout on the sustained phase of sLTP. It is possible that MMP-9 KO mice have some compensatory mechanisms and lack of MMP-9 is compensated for example by activity of another MMP. Additionally, even though MMP-9 KO mice are kept on C57BL/6 background and the line is maintained by breeding heterozygotes together, WT littermates which has been used in the study have markedly lower increase of spine volume in comparison to slices prepared from wildtype C57BL/6J mice (Fig 1). Therefore, the difference in sLTP phenotypes may be explained by some unaccounted genetic differences between the two mouse lines. It has been recently shown that even closely-related mice substrains C57BL/6J and C57BL/6N express substantial metabolic and genetic differences (Nemoto *et al*, 2022).

This early signaling by MMP-9 during sLTP apparently contradicts with previous studies suggesting that MMP-9 is required for late-phase LTP, but not for early-phase LTP (Nagy *et al*, 2006; Gorkiewicz *et al*, 2015; Wiera *et al*, 2017). Interestingly, in the paper of Nagy *et al*, 2006, LTP in MMP-9 KO animals are impaired in both early- and late-LTP, but the use of chemical inhibitors of MMP-9 affected only late-LTP. While both Gorkiewicz *et al*. (2015) and Wiera *et al*. (2013, 2017) reported impairment of only late-LTP, the study of Gorkiewicz et al. was done in amygdala and Wiera *et al*.(2013) on mossy fiber-CA3 pathway where LTP is mostly presynaptic and independent on NMDA receptors (Nicoll & Schmitz, 2005). Their observed effects of MMP-9 KO on sLTP are in agreement with our data showing a rapid MMP-9 release upon synaptic stimulation (Fig. 2) and fast activation of TrkB (Fig. 3). Both these effects might be explained by the release of the enzyme which was already accumulated at the postsynaptic site. This hypothesis may appear contradictory to the previous findings that MMP-9 is locally translated in response to synaptic stimulation and then released to contribute to the synaptic plasticity, the processes that require minutes to occur (Dziembowska *et al*, 2012; Michaluk *et al*, 2007; Stawarski *et al*, 2014). It should be, however, noted that there have been previous reports showing an expression of MMP-9 protein within the dendritic spines under the basal condition (Wilczynski *et al*, 2008; Michaluk *et al*, 2007; Aujla & Huntley, 2014). Interestingly, MMP-9 protein was

predominantly found in small dendritic spines which are more prone for plastic changes (Kasai *et al*, 2010). Additionally, differences in LTP-evoking protocols might also explain why the effect of MMP-9 inhibition on the transient phase of sLTP has not been observed before. Wang and co-workers (2008) have shown that MMP-9 is both necessary and sufficient to drive spine enlargement and synaptic potentiation concomitantly by using theta-stimulation-induced LTP paired with a depolarization of postsynaptic neurons. This pairing protocol, due to backpropagating action potential and presynaptic activation, can itself lead to the postsynaptic or presynaptic exocytotic release of BDNF and MMP-9. Therefore the glutamate action on the postsynaptic receptors in releasing those molecules could not be defined. In contrast, our single spine sLTP protocol provided direct evidences that BDNF and MMP-9 plays a role in spine-specific signaling events. Moreover, a recent paper of Stein *et al*, (2021) dissociated the NMDAR-dependent structural and functional LTP by pointing to the role of non-ionotropic NMDAR signaling through p38 MAPK. This report might further explain the differences in the kinetics of MMP-9 involvement in electrophysiological and imaging LTP experiments.

Our results showed that MMP-9 can be rapidly released upon stimulation (Fig. 2), which further supports the early action of this protease for sLTP induction. Importantly, we compared changes in fluorescence intensity of MMP9-SEP and mCherry (morphological marker) in activated spines between uncaging pulses, and these data indicate that spine volume increase alone cannot explain the observed changes in SEP fluorescence. Therefore, we infer that observed fluorescence increase is related to exocytosis events in the dendritic spine. Presented results suggest that MMP-9 release may occur within 2 seconds after the first uncaging pulse, sustained over 40 seconds, followed by a decrease to the baseline level, which may be due to the depletion of spine vesicles. The timescale of MMP-9 release is thus similar to that of BDNF release (Harward *et al*, 2016) and AMPA receptors (Patterson *et al*, 2010), suggesting that the initial phase of sLTP involves a rapid increase in various exocytosis activity.

To date, there have not been many identified ECM substrates of MMP-9 in the brain. On the other hand, post-synaptically-originating or trans-synaptic cell adhesion molecules, such as ICAM-5 (Conant *et al*, 2010), β-dystroglycan (Michaluk *et al*, 2007), nectin-3 (Van Der Kooij *et al*, 2014), CD44 (Bijata *et al*, 2017) or neuroligin-1 (Peixoto *et al*, 2012) have been shown to be partially cleaved by MMP-9. Similarly, MMP-9 has been shown to be capable to cleave proBDNF into its mature form (mBDNF) (Hwang *et al*, 2005; Mizoguchi *et al*, 2011). Mizoguchi et al. (2011) has shown that pentylenetetrazole kindling of mice over several days increases a proportion of mature to proBDNF, and this effect was diminished in MMP-9 KO animals. Additionaly, Hwang et al. (2005) incubated membrane fraction of cortical culture overexpressing proBDNF with high concentration of recombinant MMP-9 and observed proBDNF cleavage to mBDNF. To complement the existing knowledge, we showed directly the cleavage of proBDNF to mBDNF by MMP-9 without other proteases that could participate in the process or without the presence of TIMPs in the samples which might interfere with cleavage by MMPs. The presented results further support the MMP-9 involvement on BDNF maturation by demonstrating a detailed time-course of MMP-9 activity

at the excitatory synapse and the contribution of this protease to TrkB activation. Thus, our study gives insights into the ongoing discussion whether BDNF is released from dendrites in its mature- or pro-form (Sasi *et al*, 2017).

Our results of TrkB activation (Figure 3) may suggest that it is released in both molecular forms. Decreased MMP-9 activity either by application of chemical inhibitor or gene knockout leads to a decreased level of TrkB activation during the transient phase of sLTP. Furthermore, while under the control condition, the receptor activation is sustained (~ 10 min. after activation), under an MMP-9 inhibition, it reverses back to the baseline. It is possible that mBDNF is released quickly during stimulation and binds TrkB immediately (Matsumoto *et al*, 2008). In contrast, proBDNF is released later because of the repetitive nature of sLTP protocol, and requires time to be activated by MMP-9. This might also explain why previous reports have found MMP-9 role in late- rather than early-LTP.

Given that the release kinetics of BDNF and MMP-9 are similar, one could speculate that the effect of MMP-9 inhibition on early TrkB activation can be achieved because both, MMP-9 and BDNF are co-localized and co-released from the same release vesicles. This would provide spatiotemporal coordination for proBDNF cleavage by MMP-9.

Overall, our data provide insights into the pivotal role of MMP-9 in synaptic plasticity and associated TrkB activation, demonstrating rapid (seconds) MMP-9 availability and activity. In addition, we provide a molecular link between the activity of the protease and function of BDNF, by following the activity of its receptor, TrkB.

Methods

Animals

All animal procedures were approved by the Max Planck Florida Institute for Neuroscience, and Use Committees and were conducted in accordance with the NIH Guide for the Care and Use of Laboratory Animals. In this study we used 4-8 days-old mice of either sex. C57BL/6J mice were obtained from Charles River and MMP-9 KO (B6.FVB(Cg)-Mmp9tm1Tvu/J) were purchased from Jackson Laboratory. MMP-9 KO mice has been maintain by mating heterozygotes with heterozygotes. The genotype of each animal used was verified before preparing slices using PCR of genomic DNA isolated from the tail. For experiments we used MMP-9 KO mice and their wild-type (WT) littermates.

Plasmids

pCAG_GFP, pCAG_mCherry, pCAG_MMP-9 – full length mouse (MMP-9) from pcDNA3.1_MMP-9-HA (Addgene #121172) cloned into pCAG vector, pCAG_MMP-9a1205c - full length mouse MMP-9 with point mutation in single nucleotide 1205 from adenine to cytosine resulting in codon change E402A which results in lack of MMP-9 enzymatic activity. Primers used for mutagenesis: Fwd: 5'-TGGCAGCGCACGCGTTCGGCCATGC, Rev: 5'-GCATGGCCGAACGCGTGCGCTGCCA, primers used for NEBuilder HiFi DNA Assembly: Fwd: 5; tgtctcatcattttggcaagGTGGTGGAATTCATGAGTC, Rev: 5' tgctcaccatAGCGTAATCTGGAACATC.pCAG_MMP-9a1205c-SEP, SEP obtained by PCR reaction and cloned into pCAG_MMP-9a1205c vector with a use of NEBuilder HiFi DNA Assembly. Pimers: Fwd: 5' CCATACGATGTTCCAGATTACGCTATGAGTAAAGGAGAAGAACTTTTCACTGG, Rev: 5' GTTTAAACGGGCCCTCTAGACTCGAGCGGCCGCTTATTTGTATAGTTCATC For pCAG_MMP9a1205c-Gamillus, Gamillus obtained by PCR reaction from (Addgene #124837) was inserted in place of SEP with a use of NEBuilder HiFi DNA Assembly. Primers: Fwd: 5'-agattacgctATGGTGAGCAAGGGCGAG, Rev: 5': ggcagagggaaaaagatccgGCAGAATTCTTACTTGTACAGCTCG. pCAG_mCherry-Tetx obtained by Yasuda Laboratory[21]. pCAG_TrkB-GFP –Tropomyosin receptor kinase B conjugated with GFP at C terminus acting as FRET (Förster resonance energy transfer) donor for PLC RFP, pCAG_PLC-RFP – SH2 domain of phospholipase Cγ1 (PLC- γ1) conjugated with two mRFP1 at its N and C terminus acting as acceptor for TrkB FRET sensor.

Recombinant, inactive MMP-9(E402A) production

Expression of the previously described(Michaluk *et al*, 2011) recombinant non-active mutant of MMP-9(E402A) was performed using the Bac-to-Bac Baculovirus expression system, according to the manufacturer's instructions (Thermo Fisher Scientific). Briefly, DH10Bac competent cells, were transformed with pFastBac1_MMP-9(E402A) mutant was transform. Colonies that performed transposition of recombinant plasmid fragment into bacmid DNA were identified by blue–white selection, and recombinant bacmid was isolated and verified by PCR. The Sf21 insect cells were transfected with recombinant bacmid using Cellfectin reagent (Thermo Fisher Scientific) to obtain recombinant baculovirus. After amplification and titration of the recombinant baculovirus, High-Five cells were infected and incubated in the Sf-900IISFM serum-free medium (Thermo Fisher Scientific). Conditioned medium was

collected 48 hours after infected, medium was collected and MMP-9(E402A) was purified by affinity chromatography with gelatin–Sepharose 4B (Cytiva) as previously described(Sadatmansoori *et al*, 2001). Protein concentrations in the collected fractions were measured using Bradford reagent (Sigma).

proBDNF digestion assay

Twenty ng of recombinant proBDNF (Alomone Labs) was incubated with 50 ng of recombinant MMP-9 (Calbiochem) or 50 ng of recombinant, human, inactive MMP-9(E402A) in total volume of 20 µl. All reactions were incubated in reaction buffer (final concentration: 150 mM NaCl, 10 mM $CaCl_2$, 0.01% BSA, 50 mM Tris-Cl, pH7.5) for 16 hours at 30°C.

Western blotting

ProBDNF digestion samples were run on 15% SDS-PAGE gels and electro-transferred onto polyvinylidene difluoride membrane (Immobilon-P, Millipore), using semi-dry method. Membranes were blocked for 2 hours at room tempertaure with 10% (w/v) dried non-fat milk powder in Tris-buffered saline with 0.1% Tween 20 (TBS-T). After blocking, the membranes were incubated at 4°C overnight with rabbit anti-BDNF antibody (Santa Cruz) diluted 1:500 in 5% (w/v) non-fat milk in TBS-T. Membranes were then incubated for 2 hours at room temperature with horseradish-peroxidase-labelled secondary antibody (Goat Anti-Rabbit IgG Antibody; Vector Laboratories) diluted 1:10,000 in 5% dried non-fat milk powder in TBS-T. After washing, the peroxidase activity was visualized on photographic film with ECL Prime Western Blotting Detection Reagent (Cytiva). The developed film was later digitized on ChemiDoc MP Imaging System (Bio-Rad) and analyzed using Image Lab software (Bio-Rad).

Hippocampal organotypic culture and transfection

Hippocampal organotypic cultures were prepared from postnatal day 4-8 old mouse pups (either C57BL/6J or MMP-9 KO and their WT littermates). Hippocampi were dissected and sliced into 350 um thick transverse slices with a use of McIlwain tissue chopper and placed on PTFE membranes (Millicell; Merck, Cat# PICMORG50). Cultures ware kept in the air-medium interphase; medium composed of Minimal Essential Medium supplemented with, 20% heat inactivated horse serum, 12.9 mM D-Glucose, 5.2 mM $NaHCO_3$, 30mM HEPES buffer, 2 mM $MgSO_4$, 1 mM L-glutamate, 1 mM $CaCl_2$, 0.075% Ascorbic Acid and 1 µg/ml insulin. Half of media volume was exchanged every 2-3 days. After 8-13 day in culture, slices were transfected using GeneGun (BioRad) method (Woods & Zito, 2008). Gene gun bullets were prepared with plasmids pCAG_GFP 30 µg DNA (structural change experiments); pCAG_MMP-9a1205cSEP and pCAG_mCherry ratio 1:1 50 µg DNA, or pCAG_MMP9a1205cGamillus with pCAG_mCherry ration 1:1, 50 µg DNA (MMP-9 release experiments). For experiments with blocked autocrine vesicular release – by co-expression of the tetanus toxin light chain (TeTx), pCAG_MMP9a1205cSEP was mixed with pCAG_mCherry-IRES-TeTx 1:1 50 µg of DNA; pCAG TrkB GFP and pCAG PLC RFP in ratio 1:3 50 ug DNA (TrkB activation experiment). Neurons expressing GFP and MMP-9

SEP/Gamillus with mCherry were imaged 1-7 days after transfection. Neurons expressing TrkB were imaged within 12-48h from the transfection.

Two-photon FLIM

FRET measurements using a custom-built two-photon fluorescence lifetime imaging microscope was performed as previously described (Harward *et al*, 2016). GFP fluorophore was excited with 1.2-1.5 Mw, 920nm pulsating tunable laser (Ti-sapphire laser, Coherent, Cameleon). Emitted light was collected through 60x water immersion objective (NA 0.9, Olympus), split with a dichroic mirror (565 nm) and photons were detected by two separate photoelectron multiplier tubes (PMTs; H7422-40p, Hamamatsu). For green channel, light arriving to the PMT was filtered with a band-pass filter (510/70, Chroma) and for red channel using band-pass filter(620/90, Chroma). Fluorescence lifetime images were obtained using a time correlated single photon counting board (Time-harp 260, Pico-Quant) and processed by custom software FLIMage (https://github.com/ryoheiyasuda/FLIMage_public). Images for volume change measurements and TrkB activation were collected at 128x128 pixels with 7.8 Hz rate with 24 frame averaging. For MMP-9 SEP release imaging 64x64 pixels frames were collected with an 8.8 Hz rate with no averaging.

Two-photon glutamate uncaging

A second Ti-sapphire tunable laser (Coherent, Cameleon) was set to 720 nm and used to uncage 4-Methoxy-7-nitroindolinyl-caged-L-glutamate (MNI-caged glutamate, Tocris). Up to four spines in separate regions of interest (ROI) per cell were stimulated simultaneously on four distinct secondary apical dendrites. Stimulation protocol consists of train of 6 ms, 2.7-3 mW pulses (30 times at 0.5 Hz) near a spines of interest.

Organotypic hippocampal slices were imaged in Mg^{2+}-free ACSF solution (127 mM NaCl, 2.5 mM KCl, 4 mM $CaCl_2$, 25 mM $NaHCO_3$, 1.25 mM NaH_2PO_4 and 25 mM glucose) containing 1 µM tetrodotoxin (TTX, Tocris) and 2 mM MNI-caged L-gulatmate buffered with carbogen (5% CO_2 and 95% O_2). Experiments were performed at room temperature (around 24°C).

Spine volume change measurements

Spines of GFP-expressing pyramidal neurons in CA1 subfield of hippocampus were imaged sequentially up to 4 spines located on separate secondary apical dendrites. For treatment, Slices were perfused in ACSF (see above) with either DMSO (for control; final concentration 0.08%), GM6001 (Cat: 364205, Calbiochem) in DMSO final concentration 25 µM or MMP-9/MMP-13 Inhibitor I (Cat: 444252, Calbiochem) in DMSO final concentration 5 µM. Experiments were repeated on organotypic cultures from at least three different dissections.

Two-photon FLIM data analyses.

The analysis of TrkB sensor activation was performed as previously described(Harward *et al*, 2016). To measure the fraction of a donor bound to an acceptor, we fit a fluorescence lifetime curve summing all pixels over a whole image with a double exponential function convolved with the Gaussian pulse response function:

$$F(t) = F_0[P_D H(t, t_0, \tau_D, \tau_G) + P_{AD} H(t, t_0, \tau_{AD}, \tau_G)]$$

where τAD is the fluorescence lifetime of donor bound with acceptor, P_D and P_{AD} are the fraction of free donor and donor bound with acceptor, respectively, and H(t) is a fluorescence lifetime curve with a single exponential function convolved with the Gaussian pulse response function:

$$H(t, t_0, \tau_D, \tau_G) = \frac{1}{2}\exp\left(\frac{\tau_G^2}{2\tau_D^2} - \frac{t - t_0}{\tau_D}\right)\mathrm{erfc}\left(\frac{\tau_G^2 - \tau_D(t - t_0)}{\sqrt{2}\tau_D \tau_G}\right)$$

in which τ_D is the fluorescence lifetime of the free donor, τ_G is the width of the Guassian pulse response function, F_0 is the peak fluorescence before convolution and t_0 is the time offset, and erfc is the error function. We fixed τ_D to the fluorescence lifetime obtained from free eGFP (2.6 ns). To generate the fluorescence lifetime image, we calculated the mean photon arrival time, ⟨t⟩, in each pixel as:

$$\langle t \rangle = \int tF(t)dt / \int F(t)dt$$

then, the mean photon arrival time is related to the mean fluorescence lifetime, ⟨τ⟩, by an offset arrival time, t_0, which is obtained by fitting the whole image:

$$\langle \tau \rangle = \langle t \rangle - t_0$$

For small regions-of-interest (ROIs) in an image (spines or dendrites), we calculated the binding fraction (P_{AD}) as:

$$P_{AD} = \tau_D(\tau_D - \langle \tau \rangle)(\tau_D - \tau_{AD})^{-1}(\tau_D + \tau_{AD} - \langle \tau \rangle)^{-1}$$

TrkB activation

Images were collected simultaneously for up to 4 ROI located on distinct secondary apical dendrites of CA1 pyramidal neurons co-expressing TrkB-GFP and PLC-RFP constructs. Cells included in experiment had average initial binding fraction not higher than 45%. Slices were treated with either DMSO or Inhibitor I as described above. Experiments were repeated on organotypic cultures from at least three different dissections.

MMP-9 release 2P imaging

Spines were imaged sequentially from distinct proximal secondary dendrites of pyramidal cells in CA1 co-expressing MMP9-SEP and mCherry or MMP-9 Gamillus and mCherry.

Data analysis

Spine volume change was calculated using formula $\Delta F/F_0 = (F-F_0)/F_0$ where F is a sum of fluorescence in a given time from the ROI containing the spine of the interest and F_0 represents average of F from the baseline of first 5-7 time points (before sLTP protocol).

MMP-9 SEP release was calculated using traces from 13 spines, where normalized intensity was calculated using formula $\Delta F/F_0 = (F-F_0)/F_0$, where F_0 corresponds to average of frame preceding the uncaging pulse and frame of uncaging pulse. Later the results from uncaging pulses 2-18 were averaged. Same analysis was performed for data collected from red channel corresponding to cytoplasmic mCherry treated as spine volume.

Binding fraction (P_{AD}) was normalized by subtracting averaged baseline binding fraction (P_{AD0}; before sLTP protocol) with a formula $P_{AD} – P_{AD0}$.

Acknowledgements

This study was supported by National Science Centre MAESTRO grant 2017/26/A/NZ3/00379 to L. K.;. D. L. was supported by Polish National Agency for Academic Exchange, Iwanowska Fellowship, NIH (R01MH080047, R35NS116804) to R.Y.

Author contributions

Conceptualization, L.K. and P.M.; Methodology, R.Y.; Software, R.Y.; Investigation, D.L., B.K.; Writing – Original Draft, P.M.; Writing – Review & Editing, P.M., L.K., R.Y. and D.L; Visualization, P.M. and D.L.; Funding Acquisition, L.K., R.Y. and D.L.; Resources, L.K., K.K. and R.Y.; Supervision, P.M., L.K., K.K. and R.Y.

Disclosure and competing interest statement

R.Y. is a founder of Florida Lifetime Imaging LLC.

Data Availability Section

This study includes no data deposited in external repositories.

References and Citations

Aujla PK & Huntley GW (2014) Early postnatal expression and localization of matrix metalloproteinases-2 and -9 during establishment of rat hippocampal synaptic circuitry. *J Comp Neurol* 522: 1249–1263

Bajor M, Michaluk P, Gulyassy P, Kekesi AK, Juhasz G & Kaczmarek L (2012) Synaptic cell adhesion molecule-2 and collapsin response mediator protein-2 are novel members of the matrix metalloproteinase-9 degradome. *J Neurochem* 122: 775–788

Bijata M, Labus J, Guseva D, Stawarski M, Butzlaff M, Dzwonek J, Schneeberg J, Böhm K, Michaluk P, Rusakov DA, *et al* (2017) Synaptic Remodeling Depends on Signaling between Serotonin Receptors and the Extracellular Matrix. *Cell Rep* 19: 1767–1782

Borczyk M, Śliwińska MA, Caly A, Bernas T & Radwanska K (2019) Neuronal plasticity affects correlation between the size of dendritic spine and its postsynaptic density. *Sci Rep* 9: 1–12

Bozdagi O, Nagy V, Kwei KT & Huntley GW (2007) In vivo roles for matrix metalloproteinase-9 in mature hippocampal synaptic physiology and plasticity. *J Neurophysiol* 98: 334–344

Chang JY, Nakahata Y, Hayano Y & Yasuda R (2019) Mechanisms of Ca2+/calmodulin-dependent kinase II activation in single dendritic spines. *Nat Commun* 10: 1–12

Cieplak P & Strongin AY (2017) Matrix metalloproteinases – From the cleavage data to the prediction tools and beyond. *Biochim Biophys Acta - Mol Cell Res* 1864: 1952–1963 doi:10.1016/j.bbamcr.2017.03.010

Colgan LA, Hu M, Misler JA, Parra-Bueno P, Moran CM, Leitges M & Yasuda R (2018) PKCα integrates spatiotemporally distinct Ca 2+ and autocrine BDNF signaling to facilitate synaptic plasticity. *Nat Neurosci* 21: 1027–1037

Conant K, Wang Y, Szklarczyk A, Dudak A, Mattson MP & Lim ST (2010) Matrix metalloproteinase-dependent shedding of intercellular adhesion molecule-5 occurs with long-term potentiation. *Neuroscience* 166: 508–521

Cunha C, Brambilla R & Thomas KL (2010) A simple role for BDNF in learning and memory? *Front Mol Neurosci* 3: 1

Dean C, Liu H, Dunning FM, Chang PY, Jackson MB & Chapman ER (2009) Synaptotagmin-IV modulates synaptic function and long-term potentiation by regulating BDNF release. *Nat Neurosci* 12: 767–776

Dziembowska M, Milek J, Janusz A, Rejmak E, Romanowska E, Gorkiewicz T, Tiron A, Bramham CR & Kaczmarek L (2012) Activity-dependent local translation of matrix metalloproteinase-9. *J Neurosci* 32: 14538–14547

Ethell IM & Ethell DW (2007) Matrix metalloproteinases in brain development and remodeling: Synaptic functions and targets. *J Neurosci Res* 85: 2813–2823

Fields GB (2015) New strategies for targeting matrix metalloproteinases. *Matrix Biol* 44–46: 239–246 doi:10.1016/j.matbio.2015.01.002

Gorkiewicz T, Balcerzyk M, Kaczmarek L & Knapska E (2015) Matrix metalloproteinase 9

(MMP-9) is indispensable for long term potentiation in the central and basal but not in the lateral nucleus of the amygdala. *Front Cell Neurosci* 9: 73

Gorkiewicz T, Szczuraszek K, Wyrembek P, Michaluk P, Kaczmarek L & Mozrzymas JW (2010) Matrix Metalloproteinase-9 reversibly affects the time course of NMDA-induced currents in cultured rat hippocampal neurons. *Hippocampus* 20: 1105–1108

Harward SC, Hedrick NG, Hall CE, Parra-Bueno P, Milner TA, Pan E, Laviv T, Hempstead BL, Yasuda R & McNamara JO (2016) Autocrine BDNF-TrkB signalling within a single dendritic spine. *Nature* 538: 99–103

Hayashi Y (2022) Molecular mechanism of hippocampal long-term potentiation – Towards multiscale understanding of learning and memory. *Neurosci Res* 175: 3–15 doi:10.1016/j.neures.2021.08.001

Hedrick NG, Harward SC, Hall CE, Murakoshi H, McNamara JO & Yasuda R (2016) Rho GTPase complementation underlies BDNF-dependent homo- and heterosynaptic plasticity. *Nature* 538: 104–108

Huntley GW (2012) Synaptic circuit remodelling by matrix metalloproteinases in health and disease. *Nat Rev Neurosci* 13: 743–757

Hwang JJ, Park MH, Choi SY & Koh JY (2005) Activation of the Trk signaling pathway by extracellular zinc. Role of metalloproteinases. *J Biol Chem* 280: 11995–12001

Kaminari A, Giannakas N, Tzinia A & Tsilibary EC (2017) Overexpression of matrix metalloproteinase-9 (MMP-9) rescues insulin-mediated impairment in the 5XFAD model of Alzheimer's disease. *Sci Rep* 7: 1–12

Kang H, Welcher AA, Shelton D & Schuman EM (1997) Neurotrophins and time: Different roles for TrkB signaling in hippocampal long-term potentiation. *Neuron* 19: 653–664

Kasai H, Hayama T, Ishikawa M, Watanabe S, Yagishita S & Noguchi J (2010) Learning rules and persistence of dendritic spines. *Eur J Neurosci* 32: 241–249

Van Der Kooij MA, Fantin M, Rejmak E, Grosse J, Zanoletti O, Fournier C, Ganguly K, Kalita K, Kaczmarek L & Sandi C (2014) Role for MMP-9 in stress-induced downregulation of nectin-3 in hippocampal CA1 and associated behavioural alterations. *Nat Commun* 5: 4995

Lebida K & Mozrzymas JW (2017) Spike Timing-Dependent Plasticity in the Mouse Barrel Cortex Is Strongly Modulated by Sensory Learning and Depends on Activity of Matrix Metalloproteinase 9. *Mol Neurobiol* 54: 6723–6736

Lee R, Kermani P, Teng KK & Hempstead BL (2001) Regulation of cell survival by secreted proneurotrophins. *Science (80-)* 294: 1945–1948

Link E, Edelmann L, Chou JH, Binz T, Yamasaki S, Eisel U, Baumert M, Südhof TC, Niemann H & Jahn R (1992) Tetanus toxin action: Inhibition of neurotransmitter release linked to synaptobrevin proteolysis. *Biochem Biophys Res Commun* 189: 1017–1023

Lohof AM, Ip NY & Poo MM (1993) Potentiation of developing neuromuscular synapses by the neurotrophins NT-3 and BDNF. *Nature* 363: 350–353

Magnowska M, Gorkiewicz T, Suska A, Wawrzyniak M, Rutkowska-Wlodarczyk I, Kaczmarek L & Wlodarczyk J (2016) Transient ECM protease activity promotes synaptic plasticity. *Sci Rep* 6: 27757

Martinelli S, Anderzhanova EA, Bajaj T, Wiechmann S, Dethloff F, Weckmann K, Heinz DE, Ebert T, Hartmann J, Geiger TM, *et al* (2021) Stress-primed secretory autophagy promotes extracellular BDNF maturation by enhancing MMP9 secretion. *Nat Commun* 12: 1–17

Matsuda N, Lu H, Fukata Y, Noritake J, Gao H, Mukherjee S, Nemoto T, Fukata M & Poo MM (2009) Differential activity-dependent secretion of brain-derived neurotrophic factor from axon and dendrite. *J Neurosci* 29: 14185–14198

Matsumoto T, Rauskolb S, Polack M, Klose J, Kolbeck R, Korte M & Barde YA (2008) Biosynthesis and processing of endogenous BDNF: CNS neurons store and secrete BDNF, not pro-BDNF. *Nat Neurosci* 11: 131–133

Matsuzaki M, Ellis-Davies GCR, Nemoto T, Miyashita Y, Iino M & Kasai H (2001) Dendritic spine geometry is critical for AMPA receptor expression in hippocampal CA1 pyramidal neurons. *Nat Neurosci* 4: 1086–1092

Matsuzaki M, Honkura N, Ellis-Davies GCR & Kasai H (2004) Structural basis of long-term potentiation in single dendritic spines. *Nature* 429: 761–766

Michaluk P, Kolodziej L, Mioduszewska B, Wilczynski GM, Dzwonek J, Jaworski J, Gorecki DC, Ottersen OP & Kaczmarek L (2007) β-Dystroglycan as a target for MMP-9, in response to enhanced neuronal activity. *J Biol Chem* 282: 16036–16041

Michaluk P, Wawrzyniak M, Alot P, Szczot M, Wyrembek P, Mercik K, Medvedev N, Wilczek E, De Roo M, Zuschratter W, *et al* (2011) Influence of matrix metalloproteinase MMP-9 on dendritic spine morphology. *J Cell Sci* 124: 3369–3380

Miesenböck G, De Angelis DA & Rothman JE (1998) Visualizing secretion and synaptic transmission with pH-sensitive green fluorescent proteins. *Nature* 394: 192–195

Mizoguchi H, Nakade J, Tachibana M, Ibi D, Someya E, Koike H, Kamei H, Nabeshima T, Itohara S, Takuma K, *et al* (2011) Matrix metalloproteinase-9 contributes to kindled seizure development in pentylenetetrazole-treated mice by converting pro-BDNF to mature BDNF in the hippocampus. *J Neurosci* 31: 12963–12971

Monteggia LM, Barrot M, Powell CM, Berton O, Galanis V, Gemelli T, Meuth S, Nagy A, Greene RW & Nestler EJ (2004) Essential role of brain-derived neurotrophic factor in adult hippocampal function. *Proc Natl Acad Sci U S A* 101: 10827–10832

Nagy V, Bozdagi O & Huntley GW (2007) The extracellular protease matrix metalloproteinase-9 is activated by inhibitory avoidance learning and required for long-term memory. *Learn Mem* 14: 655–664

Nagy V, Bozdagi O, Matynia A, Balcerzyk M, Okulski P, Dzwonek J, Costa RM, Silva AJ, Kaczmarek L & Huntley GW (2006) Matrix metalloproteinase-9 is required for hippocampal late-phase long-term potentiation and memory. *J Neurosci* 26: 1923–1934

Nemoto S, Kubota T & Ohno H (2022) Metabolic differences and differentially expressed genes between C57BL/6J and C57BL/6N mice substrains. *PLoS One* 17: e0271651

Nicoll RA (2017) A Brief History of Long-Term Potentiation. *Neuron* 93: 281–290 doi:10.1016/j.neuron.2016.12.015

Nicoll RA & Schmitz D (2005) Synaptic plasticity at hippocampal mossy fibre synapses. *Nat Rev Neurosci* 6: 863–876 doi:10.1038/nrn1786

Niculescu D, Michaelsen-Preusse K, Güner Ü, van Dorland R, Wierenga CJ & Lohmann C (2018) A BDNF-Mediated Push-Pull Plasticity Mechanism for Synaptic Clustering. *Cell Rep* 24: 2063–2074

Okulski P, Jay TM, Jaworski J, Duniec K, Dzwonek J, Konopacki FA, Wilczynski GM, Sánchez-Capelo A, Mallet J & Kaczmarek L (2007) TIMP-1 Abolishes MMP-9-Dependent Long-lasting Long-term Potentiation in the Prefrontal Cortex. *Biol Psychiatry* 62: 359–362

Pang PT, Nagappan G, Guo W & Lu B (2016) Extracellular and intracellular cleavages of proBDNF required at two distinct stages of late-phase LTP. *npj Sci Learn* 1: 1–10

Patterson MA, Szatmari EM & Yasuda R (2010) AMPA receptors are exocytosed in stimulated spines and adjacent dendrites in a Ras-ERK-dependent manner during long-term potentiation. *Proc Natl Acad Sci U S A* 107: 15951–15956

Peixoto RT, Kunz PA, Kwon H, Mabb AM, Sabatini BL, Philpot BD & Ehlers MD (2012) Transsynaptic Signaling by Activity-Dependent Cleavage of Neuroligin-1. *Neuron* 76: 396–409

Penn AC, Zhang CL, Georges F, Royer L, Breillat C, Hosy E, Petersen JD, Humeau Y & Choquet D (2017) Hippocampal LTP and contextual learning require surface diffusion of AMPA receptors. *Nature* 549: 384–388

Sadatmansoori S, MacDougall J, Khademi S, Cooke LS, Guarino L, Meyer EF & Forough R (2001) Construction, Expression, and Characterization of a Baculovirally Expressed Catalytic Domain of Human Matrix Metalloproteinase-9. *Protein Expr Purif* 23: 447–452

Sasi M, Vignoli B, Canossa M & Blum R (2017) Neurobiology of local and intercellular BDNF signaling. *Pflugers Arch Eur J Physiol* 469: 593–610 doi:10.1007/S00424-017-1964-4

Shi SH, Hayashi Y, Petralia RS, Zaman SH, Wenthold RJ, Svoboda K & Malinow R (1999) Rapid spine delivery and redistribution of AMPA receptors after synaptic NMDA receptor activation. *Science (80-)* 284: 1811–1816

Shinoda H, Ma Y, Nakashima R, Sakurai K, Matsuda T & Nagai T (2018) Acid-Tolerant Monomeric GFP from Olindias formosa. *Cell Chem Biol* 25: 330-338.e7

Stawarski M, Stefaniuk M & Wlodarczyk J (2014) Matrix metalloproteinase-9 involvement in the structural plasticity of dendritic spines. *Front Neuroanat* 8: 68

Stein IS, Park DK, Claiborne N & Zito K (2021) Non-ionotropic NMDA receptor signaling gates bidirectional structural plasticity of dendritic spines. *Cell Rep* 34

Szklarczyk A, Lapinska J, Rylski M, McKay RDG & Kaczmarek L (2002) Matrix metalloproteinase-9 undergoes expression and activation during dendritic remodeling in adult hippocampus. *J Neurosci* 22: 920–930

Tønnesen J & Nägerl UV (2016) Dendritic spines as tunable regulators of synaptic signals. *Front Psychiatry* 7

Tu X, Yasuda R & Colgan LA (2020) Rac1 is a downstream effector of PKCα in structural synaptic plasticity. *Sci Rep* 10: 1–9

Vardalaki D, Chung K & Harnett MT (2022) Filopodia are a structural substrate for silent

synapses in adult neocortex. *Nature* 612: 323–327

Wang X Bin, Bozdagi O, Nikitczuk JS, Zu WZ, Zhou Q & Huntley GW (2008) Extracellular proteolysis by matrix metalloproteinase-9 drives dendritic spine enlargement and long-term potentiation coordinately. *Proc Natl Acad Sci U S A* 105: 19520–19525

Wiera G & Mozrzymas JW (2021) Extracellular metalloproteinases in the plasticity of excitatory and inhibitory synapses. *Cells* 10: 2055 doi:10.3390/cells10082055

Wiera G, Nowak D, van Hove I, Dziegiel P, Moons L & Mozrzymas JW (2017) Mechanisms of NMDA receptor- and voltage-gated L-type calcium channel-dependent hippocampal LTP critically rely on proteolysis that is mediated by distinct metalloproteinases. *J Neurosci* 37: 1240–1256

Wiera G, Wozniak G, Bajor M, Kaczmarek L & Mozrzymas JW (2013) Maintenance of long-term potentiation in hippocampal mossy fiber-CA3 pathway requires fine-tuned MMP-9 proteolytic activity. *Hippocampus* 23: 529–543

Wilczynski GM, Konopacki FA, Wilczek E, Lasiecka Z, Gorlewicz A, Michaluk P, Wawrzyniak M, Malinowska M, Okulski P, Kolodziej LR, *et al* (2008) Important role of matrix metalloproteinase 9 in epileptogenesis. *J Cell Biol* 180: 1021–1035

Woods G & Zito K (2008) Preparation of gene gun bullets and biolistic transfection of neurons in slice culture. *J Vis Exp*: e675

Figure legends

Figure 1. Spine-head enlargement during sLTP depends on MMP-9 activity.

A Experimental arrangement: GFP-expressing neuron in CA1 subfield of hippocampus. Individual spine in secondary dendrite was stimulated using sLTP protocol leading to the spine enlargement.

B Time-lapse z-integrated (z-stack) images of spines stimulated at time 0 min by sLTP protocol. Cross indicate a spot of two-photon uncaging, scale bar: 1 μm.

C Averaged time courses of changes in spine volume (measured as $\Delta F/F_0$) for spines stimulated by uncaging. Data are means ± SEM, DMSO (n = 50 spines; 27 cells, 15 animals), Inhibitor I (n = 46 spines; 21 cells, 10 animals). Grey box indicates duration of sLTP protocol.

D Statistical analysis of (C); Averaged spine volume changes for three phases: 1-3 min. (transient), 9-11 and 15-20 min. (sustained). Gray dots represent individual values for spines, bars are means ± SEM (black – DMSO, red – Inhibitor I). Repeated measures ANOVA (Time (F (1.175, 110.5) = 33.60, $p < 0.0001$); Inhibitor (F (1, 94) = 18.63, $p < 0.0001$); Time□Inhibitor (F (2, 188) = 0.6494, $p = 0.5235$)) followed by Šidák's multiple comparison test (DMSO vs Inhibitor I at 1-3 min ($p = 0.0350$, 95% C.I. = [0.05124 to 1.863], 9-11 min ($p = 0.0002$, 95% C.I. = [0.3747 to 1.358]) and at 15-20 min ($p = 0.0002$, 95% C.I. = [0.2553 to 0.9569])).

E as in (C), but for WT (n = 44 spines; 13 cells, 7 animals) and MMP-9 KO animals (n = 51 spines; 14 cells, 7 animals).

F Statistical analysis of (E), marks as in (D). Bars are means ± SEM (black – WT, blue – MMP-9 KO). Repeated measures ANOVA (Time (F (1.463, 136.1) = 12.56, $p < 0.0001$); MMP-9 KO (F (1, 93) = 8.444, $p = 0.0046$); Time□MMP-9 KO (F (2, 186) = 3.253, $p = 0.0409$) followed by Šidák's multiple comparison test (WT vs MMP-9 KO at 1-3 min ($p = 0.0196$, 95% C.I. = [0.08769 to 1.311]).

Figure 2. MMP-9 release during sLTP.

A MMP9-SEP fluorescence is quenched by low (< 6.0) pH inside vesicles. Stimulation of the spine promotes exocytosis. Once the vesicle fuses with the cell membrane, pore opens and the acidic environment in the vesicle's lumen is neutralized (pH 7.4) allowing for observation of fluorescence of SEP.

B Time-lapse t-integrated (t-stack) images of spines stimulated by sLTP protocol – average of 10 consecutive frames collected after indicated uncaging pulses. Separate channels of MMP9-SEP and mCherry are shown. Crosses indicate a spot of two-photon uncaging, scale bar: 1 μm.

C Averaged time courses of changes in volume (measured as $\Delta R/R_0$ for mCherry channel) for spines stimulated by uncaging. Data are means ± SEM (n = 13 spines, 3 cells, 1 animal), timing of glutamate pulses during sLTP protocol are indicated by black bars.

D Averaged time courses of changes in SEP fluorescence (measured as $\Delta F/F_0$) for spines stimulated by uncaging. Data are means ± SEM (Control n = 13 spines, 3 cells, 1 animal; + AP5 n = 13 spines, 3 cells, 2 animals; + TeTx n = 12 spines, 1 cell, 1 animal), timing of glutamate uncaging laser pulses during sLTP protocol are indicated by black bars.

E Heatmap representing averaged fluorescence of MMP9-SEP in stimulated spines (n=13). Each colored rectangle represents relative fluorescence intensity of SEP. Imaging data were divided into blocks (columns) of 16 frames matching uncaging frequency, so that uncaging pulse always occurs in a second frame of the block. sLTP protocol starts after recording baseline of 7 blocks (~ 14 s) and lasts for 60 seconds (30 pulses, 0.5 Hz). White dots represent uncaging laser pulse which occurs always during the second frame in a block during sLTP-evoking protocol.

F same as (E) but for MMP9-Gamillus.

G Averaged time courses of changes in MMP9-SEP and corresponding mCherry fluorescence (measured as $\Delta F/F_0$) for spines stimulated by uncaging. The plot represents superimposed and averaged blocks of 16 frames (2.048 s) for normalized fluorescence from 2nd to 18th uncaging pulse. Data are means ± SEM (n = 13 spines, 3 cells, 1 animal), timing of glutamate uncaging laser pulses during sLTP protocol are indicated by dashed vertical line at time = 0 s.

H Peak of the uncaging-triggered change in MMP9-SEP and mCherry fluorescence (calculated as a mean of $\Delta F/F_0$ for the three subsequent frames after uncaging pulse: 0.128-0.384 s). Dots with lines represent values for individual spines for MMP9-SEP and mCherry fluorescence paired together. Bars are means. Paired t-test (t=3.149, df=12, p = 0.0084;).

I Same as in (G) but for MMP9-Gamillus (n = 13 spines, 5 cells, 2 animals).

J same as in (H) but for MMP9-Gamillus. Paired t-test (t=1.024, df=12, p = 0.3262).

Figure 3. TrkB activation depends on MMP-9 activity.

A TrkB FRET sensor schematic.

B Two-photon FLIM images of TrkB activation averaged at indicated time points. Warmer colors represent shorter lifetimes, increased binding fraction and higher TrkB activity. White cross indicate uncaging spot, scale bar: 1 μm.

C Averaged time courses of TrkB activation (measured as a change of the sensor binding fraction) for spines stimulated by uncaging. Data are means ± SEM. Grey box indicates duration of sLTP protocol.

D Statistical analysis of (C). Averaged TrkB activation (measured as a Δ Binding Fraction) for transient phase (1-3 min after sLTP induction) and sustained phase (9-11 min. after sLTP induction) in spines incubated with DMSO (n = 70 spines, 29 cells, 16 animals) or Inhibitor I (n = 49 spines, 21 cells, 10 animals). Gray dots represent individual values for spines, bars (black – DMSO, red – Inhibitor I) are means ± SEM. Repeated measures ANOVA (Time ($F(1, 117) = 11.46$, $p = 0.0010$); Inhibitor ($F(1, 117) = 10.80$, $p = 0.0013$); Time□Inhibitor ($F(1, 117) = 0.1103$, $p = 0.7403$)) followed by Šidák's multiple comparison test (DMSO vs Inhibitor I at 1-3 min ($p = 0.0113$, 95% C.I. = [0.005425 to 0.05049]) and at 9-11 min ($p = 0.0045$, 95% C.I. = [0.008394 to 0.05346])).

E Same as in (C). Averaged time courses of TrkB activation observed in spines obtained from WT, and MMP-9 KO mice.

F same as in (D). WT (black bars, n = 66 spines; 22 cells, 10 animals), MMP-9 KO (blue bars, n = 73 spines; 25 cells, 11 animals). Repeated measures ANOVA (Time $F(1, 137) = 5.084$, $p = 0.0257$; MMP-9 KO $F(1, 137) = 7.982$, $p = 0.0054$; Time□MMP-9 KO $F(1, 137) = 0.1253$, $p = 0.7238$)) followed by Šidák's multiple comparison test (WT vs MMP-9 KO at 1-3 min ($p = 0.0351$, 95% C.I.=[0.001241 to 0.04204] and at 9-11 min ($p = 0.0149$, 95% C.I. = [0.004051 to 0.04485])).

G Representative immunoblot of digestion reaction of proBDNF incubated with active MMP-9, inactive MMP-9 (E402A), or only in the reaction buffer. Arrows indicate proBDNF (~26 kDa) and mBDNF (~14 kDa).

H Quantification of three separate Western-blots of proBDNF digestion. Gray dots represent individual values of mBDNF band intensity in separate experiments and Western-blots for each experimental condition. Bars are means ± SEM. One-way ANOVA ($F(2, 6) = 20.38$, $p = 0.0021$) followed by Tukey's multiple comparisons test (Buffer vs MMP-9 $p = 0.0034$, 95% C.I. = [-213821761 to -62305372] and E402A vs MMP-9 $p = 0.0038$, 95% C.I. = [59136932 to 210653321]).

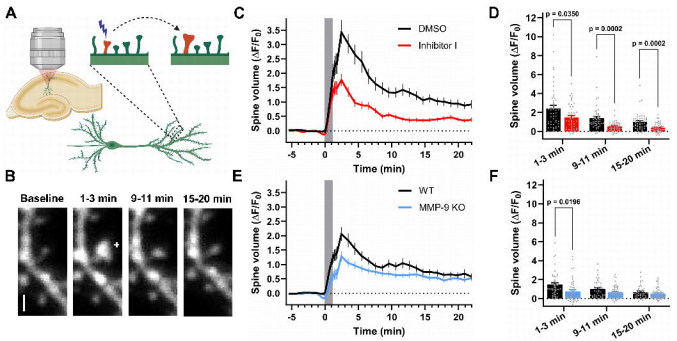
A
B
Baseline
1-3 min
9-11 min
15-20 min
C
DMSO
Inhibitor I
Spine volume (ΔF/F0)
Time (min)
D
p = 0.0350
p = 0.0002
p = 0.0002
1-3 min
9-11 min
15-20 min
E
WT
MMP-9 KO
F
p = 0.0196

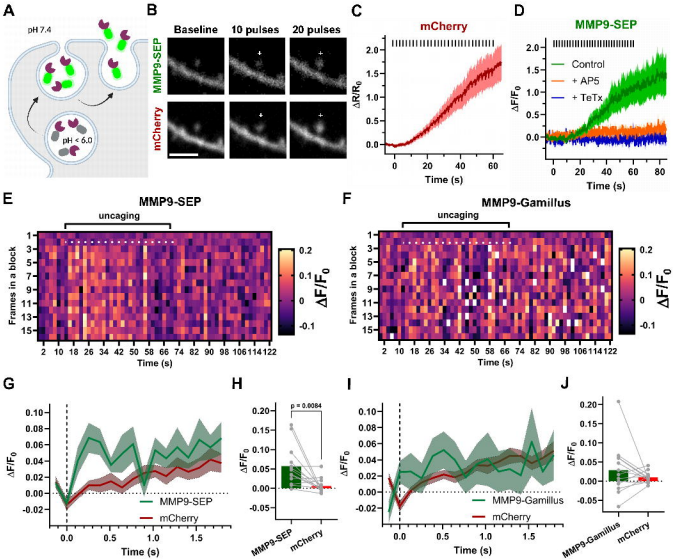
A
pH 7.4
pH < 6.0
B
Baseline
10 pulses
20 pulses
MMP9-SEP
mCherry
C
mCherry
ΔR/R0
Time (s)
D
MMP9-SEP
Control
+ AP5
+ TeTx
ΔF/F0
Time (s)
E
MMP9-SEP
uncaging
Frames in a block
ΔF/F0
Time (s)
F
MMP9-Gamillus
uncaging
Frames in a block
ΔF/F0
Time (s)
G
ΔF/F0
MMP9-SEP
mCherry
Time (s)
H
p = 0.0084
ΔF/F0
MMP9-SEP
mCherry
I
ΔF/F0
MMP9-Gamillus
mCherry
Time (s)
J
ΔF/F0
MMP9-Gamillus
mCherry

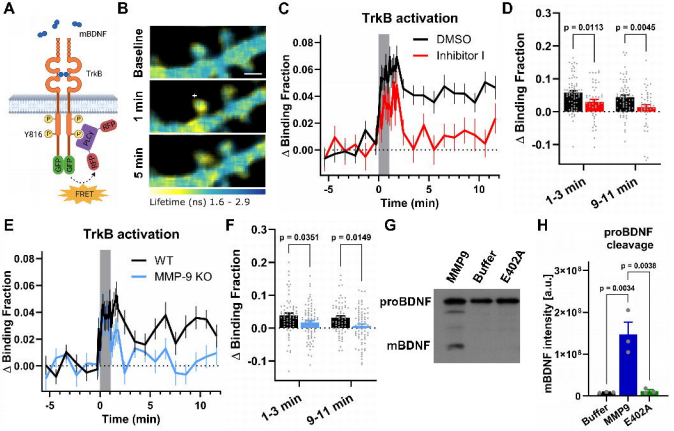
A
mBDNF
TrkB
Y816
FRET
B
Baseline
1 min
5 min
Lifetime (ns) 1.6 - 2.9
C
TrkB activation
DMSO
Inhibitor I
Δ Binding Fraction
Time (min)
D
p = 0.0113
p = 0.0046
Δ Binding Fraction
1-3 min
9-11 min
E
TrkB activation
WT
MMP-9 KO
Δ Binding Fraction
Time (min)
F
p = 0.0351
p = 0.0149
Δ Binding Fraction
1-3 min
9-11 min
G
MMP9
Buffer
E402A
proBDNF
mBDNF
H
proBDNF cleavage
p = 0.0038
p = 0.0034
mBDNF intensity [a.u.]
Buffer
MMP9
E402A